

Article

Methanation of CO₂ over Ruthenium Supported on Alkali-Modified Silicalite-1 Catalysts

Michał Zieliński , Ewa Janiszewska , Adrianna Drewniak and Mariusz Pietrowski 

Faculty of Chemistry, Adam Mickiewicz University, Uniwersytetu Poznańskiego 8, 61-614 Poznań, Poland; adrdre@st.amu.edu.pl (A.D.); mariop@amu.edu.pl (M.P.)

* Correspondence: mardok@amu.edu.pl (M.Z.); eszym@amu.edu.pl (E.J.)

Abstract: This study focuses on the catalytic properties of ruthenium catalysts supported on modified silicalite-1 (with an MFI structure). By post-synthesis modification of silicalite-1 with solutions of alkali metal compound, a novel and cost-effective method was discovered to create basic centers on the surface of silicalite-1 supports. The modification not only affected the basicity of the supports but also their porosity. The influence of the type of alkali solution (KOH or NaOH) and its concentration (0.1 M or 1.0 M) on both the basicity and porosity was investigated. The modified silicalite-1 materials were employed as supports for ruthenium catalysts (1 wt.% Ru) and evaluated for their CO₂ methanation activity. The results were compared with the hydrogenation performance of ruthenium catalysts supported on unmodified silicalite-1. Characterization of the supports and catalysts was conducted using techniques such as BET, XRD, FT-IR, ICP-OES, TPR-H₂, H₂ chemisorption, TPD-CO₂, SEM, and TEM. Remarkably, the catalytic activity of ruthenium supported on silicalite-1 treated with 1.0 M NaOH (exhibiting selectivity toward methane above 90% in a reaction temperature range of 250–450 °C) outperformed both unmodified and KOH-modified silicalite-1 supported Ru catalysts.

Keywords: ruthenium catalyst; modified silicalite-1; surface basicity; CO₂ methanation



Citation: Zieliński, M.;

Janiszewska, E.; Drewniak, A.; Pietrowski, M. Methanation of CO₂ over Ruthenium Supported on Alkali-Modified Silicalite-1 Catalysts. *Molecules* **2023**, *28*, 6376. <https://doi.org/10.3390/molecules28176376>

Academic Editors: Yinghuai Zhu and Lin Huang

Received: 28 July 2023

Revised: 25 August 2023

Accepted: 29 August 2023

Published: 31 August 2023



Copyright: © 2023 by the authors. Licensee MDPI, Basel, Switzerland. This article is an open access article distributed under the terms and conditions of the Creative Commons Attribution (CC BY) license (<https://creativecommons.org/licenses/by/4.0/>).

1. Introduction

The expanding human activities and continuous advancement of industrial technologies greatly contribute to ongoing climate changes, with the primary cause being the increasing concentration of carbon dioxide in the atmosphere. Carbon dioxide, as a greenhouse gas, has a significant impact on amplifying the greenhouse effect. Therefore, various attempts have been made to utilize CO₂ generated from industrial processes to minimize its emissions into the atmosphere and improve the state of our environment. Significant efforts are being made to replace conventional fossil fuels with renewable energy sources such as wind or solar energy.

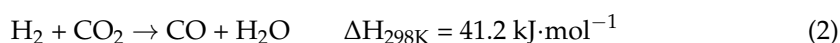
One of the main challenges associated with the growth of renewable energy production is intermittency, which requires balancing electricity generation and/or storing energy surpluses [1]. On the other hand, CO₂ emissions result in the wastage of large amounts of carbon, which is a building block for fossil fuels and petrochemical products. The most commonly utilized technology is carbon capture and storage (CCS), which involves capturing CO₂, transporting it, and storing it underground. Alternatively, captured CO₂ can be utilized and transformed into fuels and chemicals, such as dry methane reforming for synthetic gas production or CO₂ hydrogenation into methane, methanol, or higher alcohols.

The CO₂ methanation reaction was discovered by Sabatier and Senderens back in the 19th century [2]. However, currently, it is primarily utilized in research in the sustainable energy industry and is commonly found alongside hydrogen production processes (e.g., water electrolysis) in most projects. The process is known as power-to-gas technology. In power-to-gas technology, excess renewable electricity is used to produce hydrogen

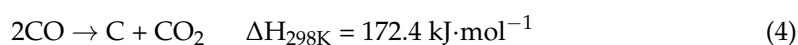
through PEM (*Proton Exchange Membrane*) electrolysis technology, which is then reacted with CO₂ to undergo a chemical transformation into methane. The hydrogenation of CO₂ to produce methane, known as the Sabatier reaction, is an exothermic reaction (1):



and is thermodynamically favorable ($\Delta G_{298\text{K}} = -130.8 \text{ kJ}\cdot\text{mol}^{-1}$). Indeed, other reactions can occur, as the weakly endothermic reverse water gas shift—RWGS (2):



or reactions involving CO (3) and (4):



Methane, as an energy carrier, can be stored for later use at a different location or time, or injected into the existing natural gas grid. This allows for the efficient storage and utilization of renewable energy, providing flexibility and balancing the intermittent nature of renewable sources.

In recent years, research has intensified regarding the acquisition of a catalyst that exhibits high activity and selectivity in this reaction, while also being resistant to high temperatures. Besides the active phase, the support material is an important component of an active and selective catalyst, and both the active phase and its support play crucial roles in catalytic process. Metal–support interactions can modify the catalytic properties of the metallic phase, thus emphasizing the significance of the support's nature in the reaction pathway [3,4]. Catalysts based on Ru, Rh, and Pd supported on different oxides (Al₂O₃, TiO₂, ZrO₂, CeO₂, or MgO) have exhibited excellent catalytic properties in CO₂ methanation [5–8], among which Ru is the most active component at low temperature [9–12].

Furthermore, it has been shown that the catalytic activity and selectivity of CO₂ hydrogenation catalysts can be improved by doping the supports with various additives, such as alkali metals (Na, K, Li, Cs) [4,13–19] and alkaline earth (Ca, Ba, Sr, Mg) [15,20,21], as well as lanthanides (La, Ce) [15].

Within the aforementioned context, the aim of this study was to use silica support with an MFI structure (silicalite-1) with varying basicity as a support for a ruthenium catalyst. The basic centers on the surface of silicalite-1 supports were created by post-synthesis modification of silicalite-1 with solutions of alkali metal hydroxides (KOH or NaOH) of different concentrations (0.1 M or 1 M). The impact of support basicity on the efficiency of the resulting ruthenium catalysts in CO₂ hydrogenation to methane was investigated. Considering the influence of support texture and basic functionality on catalyst activity, the supports and catalysts were characterized using techniques such as low-temperature nitrogen adsorption/desorption (BET), X-ray powder diffraction (XRD), Fourier-transform infrared spectroscopy (FTIR), temperature-programmed reduction with hydrogen (TPR-H₂), inductively coupled plasma optical emission spectroscopy (ICP-OES), H₂ chemisorption, temperature-programmed desorption of carbon dioxide (TPD-CO₂), scanning electron microscopy (SEM), and transmission electron microscopy (TEM). The catalytic activity of ruthenium catalysts supported on unmodified and modified silicalite-1 was compared. The effect of catalyst texture and basicity on the activity of ruthenium catalysts in the hydrogenation of CO₂ to produce methane was evaluated. To the best of our knowledge, there are no available data on such modifications of silicalite-1 followed by their application as support materials for ruthenium catalysts for hydrogenation processes.

2. Results and Discussion

The FTIR spectra (Figure 1) of the initial material (Sil) and modified silicalite-1 samples show bands typical for siliceous materials and which are insensitive to the structure (1230, 1100, 800, and 450 cm^{-1}), and a band originating from the vibration of the double five-ring of the MFI framework [22]. The presence of a band at 550 cm^{-1} in the spectra of modified samples suggests that the MFI structure was maintained after the alkaline treatment of silicalite-1. The high intensity of this band indicates good crystallinity of the modified samples [23]. Moreover, the ratio of the intensities of bands at 450 and 550 cm^{-1} for modified samples enables the calculation of their crystallinity by comparison to the ratio of these bands in unmodified silicalite-1, whose crystallinity is regarded as 100% (Table 1).

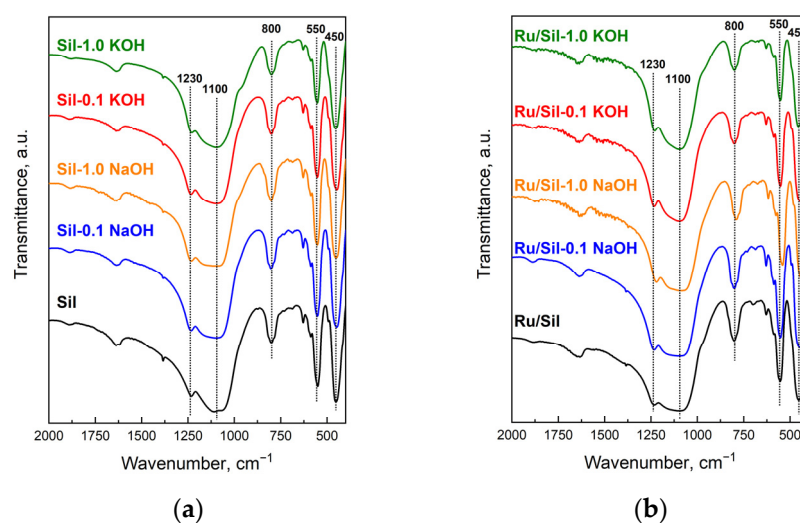


Figure 1. FTIR spectra of indicated supports (a) and catalysts (b).

Table 1. Physicochemical characterization of supports and catalysts.

Sample Symbol	$C_{\text{IR}}^{(a)}$, %	S_{BET} , $\text{m}^2 \cdot \text{g}^{-1}$	S_{ext} , $\text{m}^2 \cdot \text{g}^{-1}$	V_{tot} , $\text{cm}^3 \cdot \text{g}^{-1}$	V_{micro} , $\text{cm}^3 \cdot \text{g}^{-1}$	V_{meso} , $\text{cm}^3 \cdot \text{g}^{-1}$
Sil	100	315	82	0.19	0.12	0.07
Sil-0.1 NaOH	89	355	120	0.26	0.11	0.15
Sil-1.0 NaOH	73	299	112	0.16	0.09	0.07
Sil-0.1 KOH	83	348	164	0.26	0.09	0.17
Sil-1.0 KOH	66	181	40	0.10	0.07	0.03
Ru/Sil	86	318	111	0.16	0.06	0.10
Ru/Sil-0.1 NaOH	79	352	178	0.26	0.08	0.18
Ru/Sil-1.0 NaOH	71	290	115	0.17	0.09	0.08
Ru/Sil-0.1 KOH	74	336	186	0.24	0.07	0.17
Ru/Sil-1.0 KOH	59	202	68	0.11	0.06	0.05

^(a) C_{IR} crystallinity defined as $(I_{550}/I_{450})/0.72 \cdot 100\%$ (I_{550} and I_{450} —the intensities of the bands at 550 and 450 cm^{-1})—see Experimental Section.

The results indicate a decrease in the crystallinity of modified silicalite-1 samples in comparison to the unmodified Sil, due to the extraction of silicon species from the framework with the formation of the defects containing sodium or potassium ions. The increase in the concentration of the solution used for modification caused a higher decrease in crystallinity regardless of the used alkali compound. It is caused by the formation of a higher number of defects in the structure of silicalite-1 during modification with solutions of higher concentration. Comparing the crystallinity of the samples modified with NaOH to the crystallinity of the samples modified with KOH (for the same concentration), a higher loss of crystallinity was observed for samples modified with KOH solutions. The

crystallinity of Sil-1.0 KOH was only 66%, whereas the crystallinity of Sil-1.0 NaOH was 73%. This indicates a better tolerance for NaOH treatment than for KOH modification. The introduction of the ruthenium phase on the unmodified and modified silicalite-1 caused a further decrease in the crystallinity of the used supports. The highest loss was observed for unmodified silicalite-1 (14%). For catalysts with alkali-modified supports, a higher loss of crystallinity was observed for supports modified with an alkali solution of lower concentration, regardless of the alkali compounds used. The source of ruthenium used was ruthenium chloride and, in our previous work, we have shown that modification of silicalite-1 with NH_4Cl and NH_4OH influences the structure, causing the decrease in crystallinity [22]. This suggests that, in the conditions of impregnation used, chlorine ions present in RuCl_3 act as a structure modifier, similarly to chlorine in the procedure of modification used by NH_4Cl . On the other hand, XRD data presented below show the formation of NaCl or KCl during impregnation on supports modified with 1.0 M XOH (X = K or Na). This indicates that chlorine from RuCl_3 reacts with sodium and potassium ions present in defects formed in the framework of silicalite-1. It seems that, in this case, Na^+ and K^+ protect the structure from modification by Cl^- . The protection is higher for supports with a higher amount of alkali ions, which is equivalent to a higher amount of defects. The higher concentration of defects is present in supports modified with 1.0 M XOH, which explains their lower sensitivity to the action of chlorine during the impregnation process.

Figure 2 shows the powder X-ray diffraction (XRD) patterns of the initial silicalite-1 and the modified samples. It can be seen clearly that all supports exhibit well-resolved MFI structure peaks at $2\theta = 6\text{--}60^\circ$ [24,25]. The diffraction peaks of silicalite-1 samples modified with a solution of KOH or NaOH are slightly weaker than those of the initial silicalite-1. It indicates that the modification with an alkali solution caused a decrease in the crystallinity of silicalite-1. The decrease in crystallinity increases with the concentration of the alkali solution used for modification (Figure 2a). Comparison of the intensity of reflection for samples modified with NaOH and KOH of the same concentration indicates a higher decrease in crystallinity for samples modified with KOH solutions (Figure 2b). The obtained results of XRD analysis are in line with the FTIR data.

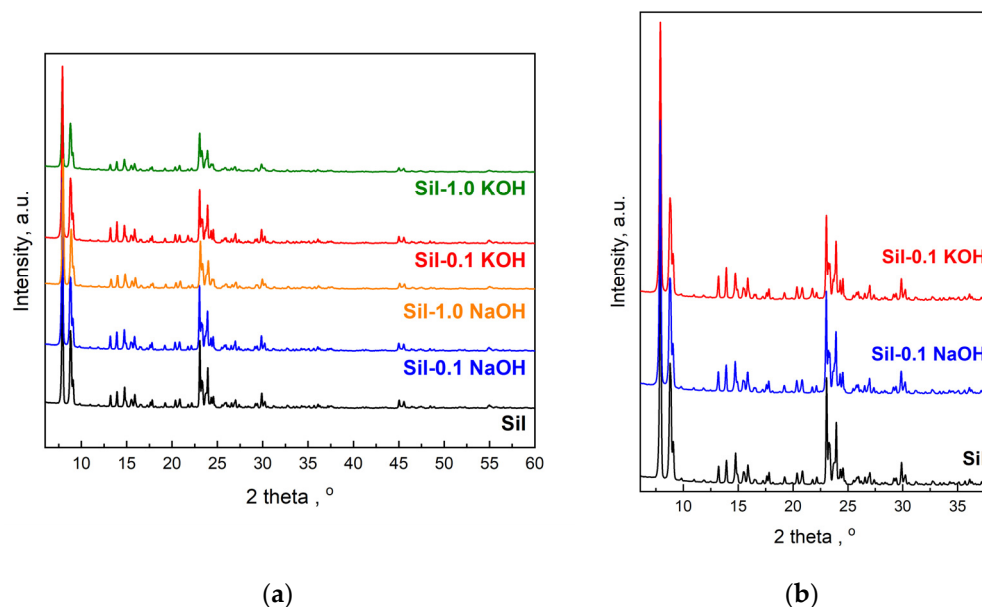


Figure 2. Comparison of XRD patterns of pristine and modified silicalite-1 samples (a) and patterns of samples modified with solutions of different alkali compounds of the same concentration (b).

The crystallinity of the catalysts is almost comparable to that of the supports (Figure 3). It indicates that the conditions of impregnation used are mild enough and do not affect the structure of the supports. Characteristic peaks of metallic Ru species ($2\theta = 44.37^\circ$) were not

observed due to the low ruthenium content (1 wt.%—determined by the ICP-OES method) as well as the high dispersion of ruthenium species on the supports. Similarly, the absence of reflections from ruthenium, at low active phase loadings, was observed by the authors of the paper [26]. Only for catalysts supported on samples modified with 1.0 M potassium and sodium solutions, additional reflection at $2\theta = 28.314^\circ$, 40.472° , and 50.127° attributed to KCl crystals (JCPDS Card number 41-1476), and $2\theta = 31.693^\circ$ attributed to NaCl crystals (JCPDS Card number 72-1668), were observed, respectively (Figure 3). This indicates the reaction of alkali ions (Na^+ and K^+) occurring in the defects with chloride ions present in the ruthenium precursor. The above-mentioned reflections are not observed in patterns of catalysts supported on Sil-0.1 NaOH and Sil-0.1 KOH due to low concentrations of sodium and potassium in these supports.

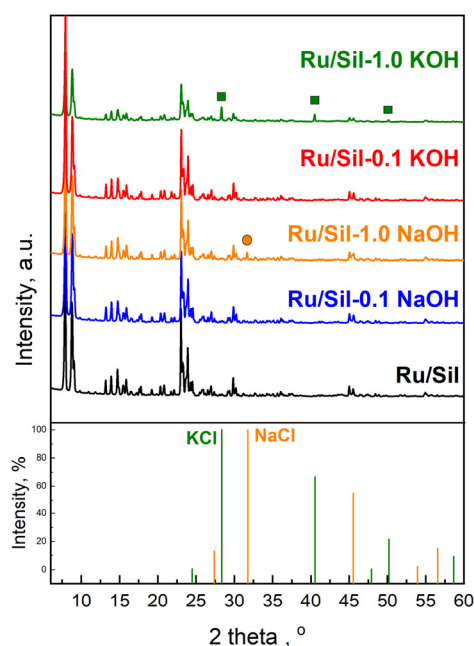


Figure 3. Comparison of XRD patterns of indicated catalyst, and NaCl and KCl.

The morphology of the original and the alkali-treated silicalite-1 was studied by scanning and transmission electron microscopies. SEM images show the influence of the type and concentration of modifiers on the morphology of the obtained supports (Figure 4a–d). The unmodified silicalite-1 (Figure 4a) possesses well-formed, separated twin crystals typical for MFI materials with a smooth surface [27].

However, the modification with 0.1 M concentration of alkali solution caused the damage of the crystals with visible detached and/or amorphous segments, as shown in Figure 4b,c. The damage of the crystals is more severe for samples modified with a higher concentration of alkali solution, and, in this case, the damaged crystals are connected in larger agglomerates (Figure 4d).

The alteration in the morphology of the crystals and the formation of additional pores after alkali modification can also be observed in the TEM images of the modified samples (Figure 5). No porosity is visible in the crystals of the initial silicalite-1 (Figure 5a), whereas the crystals of modified samples exhibit etched irregular pores. The crystals of supports modified with a 0.1 M alkali solutions (Figure 5b,c) show additional pores in the form of the channels, and the sample treated with KOH displays more open structures with larger pores, which is consistent with the data from XRD and FTIR analyses. The TEM image of the support treated with 1.0 M KOH (Figure 5d) shows the more pronounced alterations in the crystals, and the additional pores are bigger compared to the pores formed after treatment with 0.1 M solutions, and they look like holes.

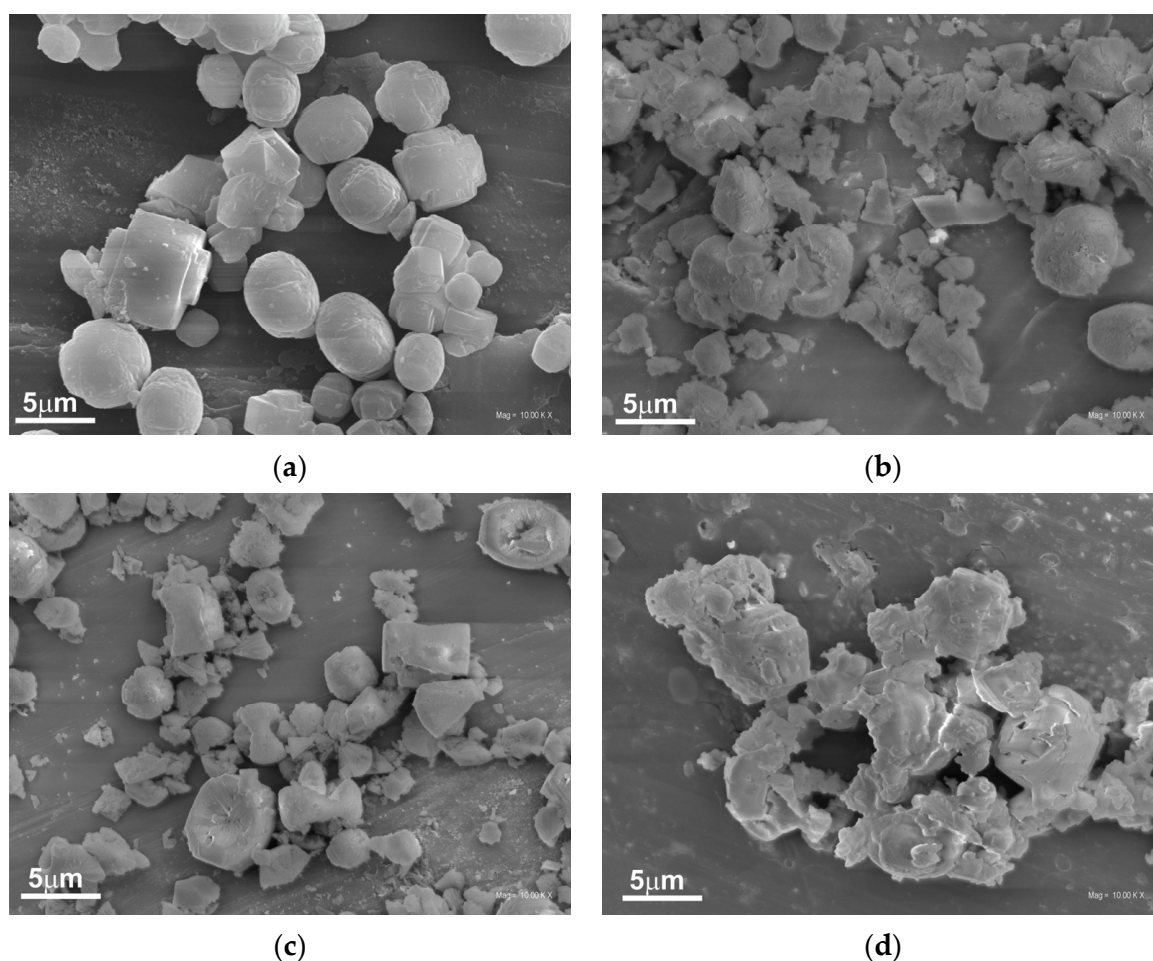


Figure 4. SEM images of the supports: Sil (a), Sil-0.1 KOH (b), Sil-0.1 NaOH (c), and Sil-1.0 KOH (d).

The textural properties of the supports and catalysts were characterized by the low-temperature nitrogen adsorption–desorption measurements. The modification of silicalite-1 with low-concentration alkali solutions resulted in an increase in specific surface area (SSA) and total pore volume, whereas modification with a more highly concentrated solution caused a decrease in these values (Table 1). The alkaline treatment of silicalite-1 also led to an increase in mesoporosity (mesopore surface area (S_{ext}) and volume (V_{meso})), accompanied by a loss of microporosity (V_{micro}). The exception is sample Sil-1.0 KOH, which shows a decrease in mesoporosity compared to the mesoporosity of the unmodified sample. This could be a result of higher degradation of the structure by modification with 1.0 M KOH, in comparison to the influence of other solutions on the structure of silicalite-1. The observed decrease in micropore volume for all modified samples is assigned to a loss of crystallinity, which is in agreement with XRD and FTIR data [28]. The introduction of the ruthenium phase on the surface of the supports practically did not change the specific surface area and total pore volume. However, differences in microporosity and mesoporosity between catalysts and supports were observed. A decrease in microporosity was observed, accompanied by an increase in mesopores, as a result of further deterioration of the silicalite-1 structure of the supports by chloride ions during the impregnation procedure. The impregnation with the ruthenium phase led to the highest drop in micropore volume on unmodified silicalite-1, whereas the lowest drop (or even no change) was observed for catalysts obtained with supports modified with 1.0 M XOH. These results are in line with the loss of crystallinity of the catalysts compared to the supports, as estimated based on the FTIR data.

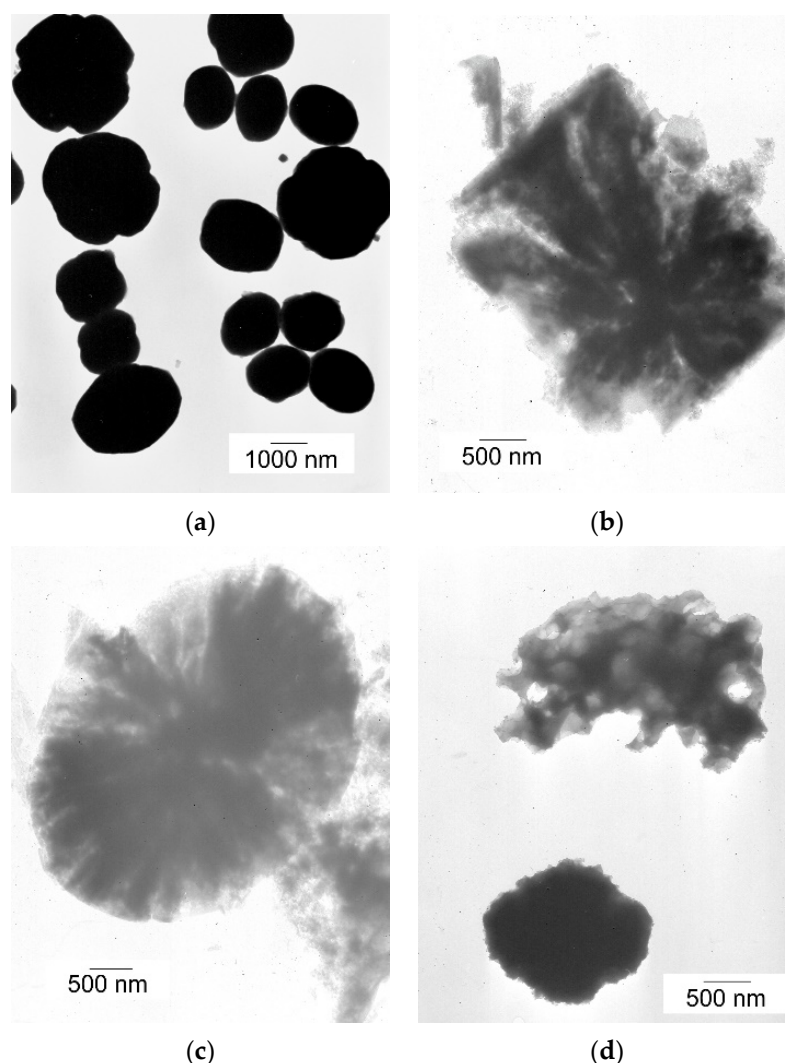


Figure 5. TEM images of unmodified (a) and modified with 0.1 M NaOH (b), 0.1 M KOH (c), and 1.0 M KOH (d) supports.

Figure 6 shows the N_2 isotherms and the corresponding pore size distribution of the supports. The isotherms of the unmodified silicalite-1, as well as modified samples, exhibit two hysteresis loops. The first one at $\sim 0.2 p/p_0$ occurs for silica MFI materials and its broadening for samples modified with 0.1 M XOH is a result of the increasing amount of defects formed during alkali modification [22,29]. Such a hysteresis loop does not change for a support modified with a 1.0 M NaOH solution. This is probably due to the low crystallinity of Sil-1.0 NaOH, and the formation of defects in the framework of this sample is balanced by its partial amorphization. In the case of Sil-1.0 KOH, amorphization predominates over defect formation, and, as a result, the low-pressure hysteresis loop disappeared. The second hysteresis loop ($p/p_0 > 0.45$) for the initial sample is attributed to the intercrystalline porosity. The increasing volume of the second loop for the samples modified with 0.1 M XOH is associated with the generation of additional mesoporosity during the applied procedure. It is illustrated by the pore distribution (Figure 6b) as the additional pores with larger diameters compared to the pores of the starting material. However, for supports modified with 1.0 M alkali solutions, the high-pressure loop disappears due to the connection of the silicalite-1 crystals into more dense, glued agglomerates during modification, as evidenced by SEM analysis (Figure 4d). The N_2 isotherms and pore size distributions for the catalysts are similar to those of the supports.

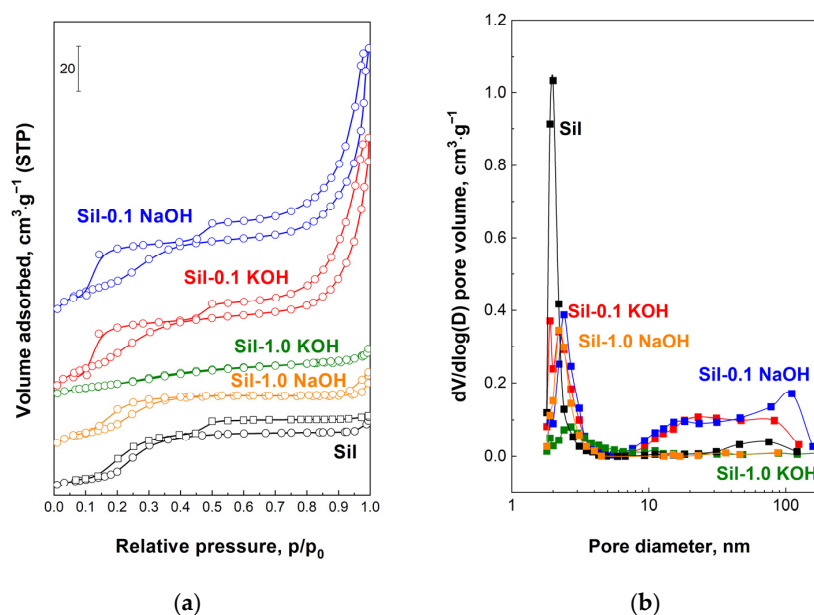


Figure 6. N₂ adsorption/desorption isotherms (a) and pore size distribution (b) for indicated supports.

To prove the effect of support modification on the nature of the basic sites, temperature-programmed desorption of CO₂ (TPD-CO₂) was conducted (Figure 7). TPD-CO₂ analysis was performed for all of the calcined supports (Figure 7a) and the catalysts (Figure 7b) that were pre-reduced in situ under H₂ at 500 °C before CO₂ adsorption at 50 °C. Table 2 reports the corresponding amounts of desorbed CO₂ calculated by integration of the relevant profiles and the density of basic sites. Only the initial, unmodified support (silicalite-1) did not show CO₂ adsorption (straight line) and its content of basic centers was 0 (Table 2). After modification with alkali metal compounds, supports exhibited CO₂ desorption dependent on the type and concentration of the modifier. Two CO₂ desorption peaks with maxima at 110 °C and in the range of 200–450 °C are attributed to weak and medium/strong CO₂ chemisorption, respectively, indicating the basic properties of the modified systems. Similarly, the presence of two types of centers were observed by Sun, et al. for Ru/CeO₂ catalysts [30] and Gao et al. [31] for La₂O₃-modified SiO₂.

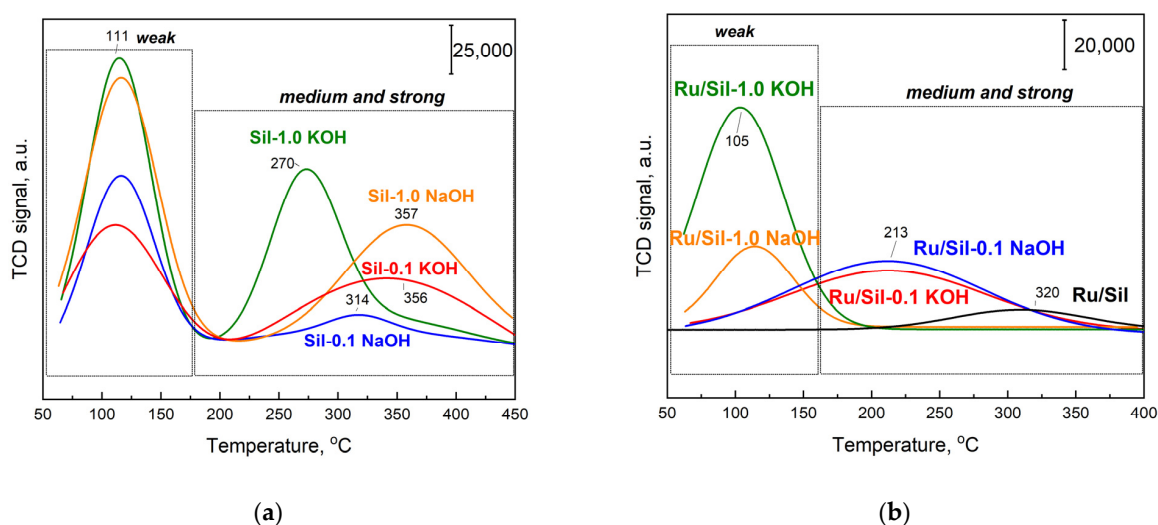


Figure 7. TPD-CO₂ profiles for supports (a) and corresponding Ru/Sil catalysts pre-reduced in H₂ at 500 °C (b); TPD-CO₂ condition: saturation at 50 °C under CO₂ flow for 60 min; heating at 10 °C/min under pure He flow.

Table 2. Amounts of CO₂ released during TPD-CO₂ tests performed on calcined support and pre-reduced catalysts.

Sample Symbol	Total Concentration of Basic Sites, $\mu\text{mol}\cdot\text{g}^{-1}$	Density of Basic Sites, $\mu\text{mol}\cdot\text{m}^{-2}$
Sil	0	0
Sil-0.1 NaOH	16.8	0.05
Sil-1.0 NaOH	46.3	0.15
Sil-0.1 KOH	14.4	0.04
Sil-1.0 KOH	51.6	0.28
Ru/Sil	4.2	0.01
Ru/Sil-0.1 NaOH	15.4	0.04
Ru/Sil-1.0 NaOH	33.4	0.12
Ru/Sil-0.1 KOH	12.9	0.04
Ru/Sil-1.0 KOH	44.1	0.23

The introduction of the Ru active phase causes the decrease in the concentration of CO₂ desorption centers for catalysts with modified supports (Figure 7b, Table 2) compared to the initial supports, whereas the concentration of centers able to adsorb CO₂ for unmodified silicalite-1 increased after the introduction of the Ru phase. This suggests that the presence of ruthenium particles on unmodified Sil generates new centers able to adsorb CO₂. The desorption maximum is present at a high temperature (~ 320 °C—Figure 7b), indicating the formation of strong adsorption centers. Similarly, Cobo et al. [32] studying modified 5% Ru/Al₂O₃ catalysts showed that CO₂ is adsorbed not only on the basic centers present on the support surface, but also on Ru sites.

The decrease in CO₂ adsorption concentration for Ru/Sil-1.0 NaOH and Ru/Sil-1.0 KOH catalysts is associated with the formation of NaCl and KCl, respectively, on their surfaces during the introduction of the active phase from RuCl₃, as confirmed by XRD studies—Figure 3. In the case of Ru/Sil-1.0 NaOH and Ru/Sil-1.0 KOH catalysts, there is a noticeable disappearance of the medium/strong centers (in the range 200–450 °C—Figure 7b), suggesting that these centers are involved in the formation of the respective chlorides, while also participating in CO₂ activation during methanation. The total amount of CO₂ desorbed was used as a metric of basic density over the catalysts (Table 2). The Ru/Sil-1.0 KOH catalyst had the highest basic density, 0.23 $\mu\text{mol m}^{-2}$, almost twice that of Ru/Sil-1.0 NaOH, 0.12 $\mu\text{mol m}^{-2}$, and almost six times more than Ru/Sil-0.1 NaOH and Ru/Sil-0.1 KOH catalysts.

To obtain information regarding the reducibility of the active phase precursor, ruthenium chloride was deposited on the investigated supports and temperature-programmed reduction with hydrogen (TPR-H₂) studies were performed. The TPR-H₂ tests were carried out for dried catalysts, and their reduction profiles are presented in Figure 8. The initial analysis of the TPR profiles of the catalysts reveals that the maxima of the active phase precursor reduction occur at different temperatures for various supports. This indicates different strengths of interactions between the precursors and the surface of individual supports and/or different precursor dispersion. Quartz sand, on which the precursor—RuCl₃·nH₂O, was deposited using the impregnation method, served as a reference in the TPR studies.

The one-step reduction process has been recorded for the RuCl₃·nH₂O standard (Ru/quartz sand) and the Ru/Sil reference catalyst, with reduction peaks at 205 and 196 °C, respectively. The one-step reduction process of the RuCl₃·nH₂O precursor to Ru was recorded, among others, by the authors of the paper [33]. They showed that direct reduction of ruthenium chloride, without calcination, favors the formation of small crystallites of the active phase. The shift in reduction temperatures towards lower values for catalysts with modified supports relative to the standard and starting Ru/Sil is related to the better dispersion of the active phase on the support. This suggests that the modification

of supports facilitates the dispersion of the active phase, resulting in smaller and more finely distributed crystallites of ruthenium, which can be beneficial for catalytic activity.

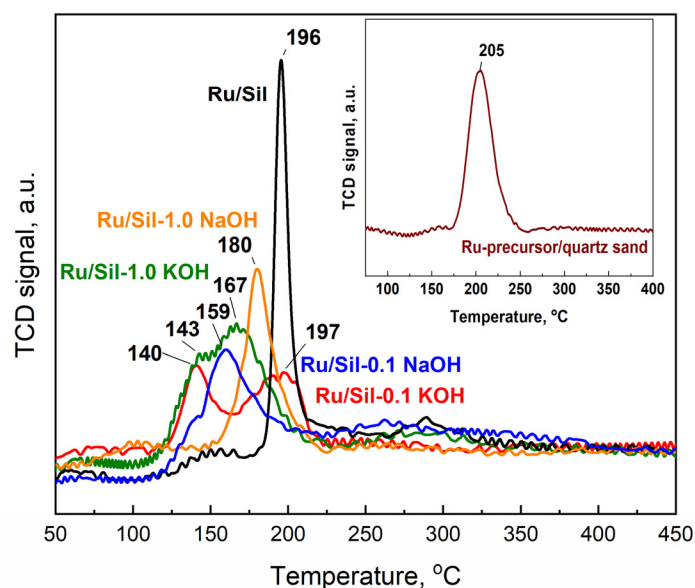


Figure 8. TPR-H₂ profiles of the dried ruthenium catalysts and RuCl₃·nH₂O precursor supported on the quartz sand (inset). Signal intensity was normalized to 100 mg.

Moreover, the reduction process of RuCl₃·nH₂O for catalysts with modified supports occurs in two steps, which is most visible in the profiles of the Ru/Sil-0.1 KOH and Ru/Sil-1.0 KOH catalysts. The reduction peaks occurred at temperatures of 140 °C and within the range of 165–200 °C, respectively. In the case of catalysts modified with a NaOH solution, two clear reduction peaks were not observed, and only slight inflections appeared on the TPR-H₂ profiles—Figure 8.

The two-step reduction corresponds to the reduction of surface Ru⁴⁺ species, formed during catalyst drying, to Ru²⁺ and then to Ru⁰, while the high-temperature analogue for the Ru/Sil catalyst corresponds to the direct reduction of the chloride precursor to metallic ruthenium. Similar reduction profiles of ruthenium catalysts were observed by the authors of [34,35] for a Ru/Al₂O₃ catalyst, Esen et al. [36] for Ru/SiO₂ or Zieliński et al. [37] for Ru/MgF₂ catalysts. The above studies indicate that the use of a modified system as a support of ruthenium facilitates its reduction process.

The TPR-H₂ results have been correlated with those obtained from hydrogen chemisorption or TEM. The ruthenium dispersion of the samples was determined by H₂ chemisorption considering a stoichiometry H/Ru = 1 [38]. From the dispersion values, an average particle size was estimated considering spherical particles. Blank experiments proved that the H₂-pretreated initial and modified supports did not adsorb hydrogen. The results of hydrogen chemisorption measurements suggest that the textural and basic properties of the supports influence the dispersion and particle size of the active ruthenium phase.

The smallest particles were observed in Ru/Sil-0.1 NaOH and Ru/Sil-0.1 KOH, with particle sizes of 2.1 (D = 50%) and 2.9 nm (D = 35.2%), respectively (Table 3). The Ru/Sil catalyst exhibited the lowest dispersion (D < 5%). The highest dispersion shows the catalysts were supported on supports modified with low concentration of alkali solution. The dispersion of the active phase was found to be three times higher for Ru/Sil-0.1 NaOH than for Ru/Sil-1.0 NaOH and almost twice for the Ru/Sil-0.1 KOH catalyst compared to dispersion of Ru/Sil-1.0 KOH. Although Ru/Sil-1.0 NaOH and Ru/Sil-1.0 KOH catalysts showed higher basicity compared to systems with 0.1 M solution-modified supports, this modification did not lead to better dispersion. The strength of the basic centers might have influenced the dispersion, in addition to their concentration. The Ru/Sil-0.1 NaOH and

Ru/Sil-0.1 KOH catalysts exhibited basic center strengths in the medium/strong range, while the Ru/Sil-1.0 NaOH and Ru/Sil-1.0 KOH systems were in the weak range.

Table 3. Hydrogen chemisorption and CO₂ hydrogenation activity on ruthenium catalysts reduced at 500 °C.

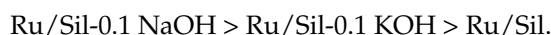
Sample Symbol	Hydrogen Chemisorption Data for Ruthenium Catalysts ^(a)					CO ₂ Methanation Rate at 450 °C mmol _{CO₂} · mmol _{Ru} ⁻¹ · s ⁻¹
	Volume Adsorbed, cm ³ · g ⁻¹			Dispersion, %	Particle Size of Ru ^(b) , nm	
	H _t	H _{irr}	H _r	D _t		
Ru/Sil	0.05	0.01	0.04	4.5	22.7	1.057
Ru/Sil-0.1 NaOH	0.55	0.11	0.44	50.0	2.1	1.903
Ru/Sil-1.0 NaOH	0.17	0.08	0.09	15.3	6.7	1.155
Ru/Sil-0.1 KOH	0.39	0.18	0.21	35.2	2.9	1.597
Ru/Sil-1.0 KOH	0.29	0.06	0.23	26.1	3.9	1.231

^(a) Dispersion and mean size of Ru particles (in nm) were determined by H₂ chemisorption at 100 °C; H_t—total adsorbed hydrogen; H_r—reversibly adsorbed hydrogen; H_{irr}—irreversibly adsorbed hydrogen; D_t—dispersion calculated from total adsorbed hydrogen. ^(b) The mean size of metal particles calculated from the amount of total chemisorbed hydrogen.

When categorizing the studied systems into two groups, modified with 1.0 M and 0.1 M solutions, we observe a clear trend in basicity. For the Ru/Sil 1.0 XOH systems, the basicity decreases similarly to the dispersion of the active phase in the following order:



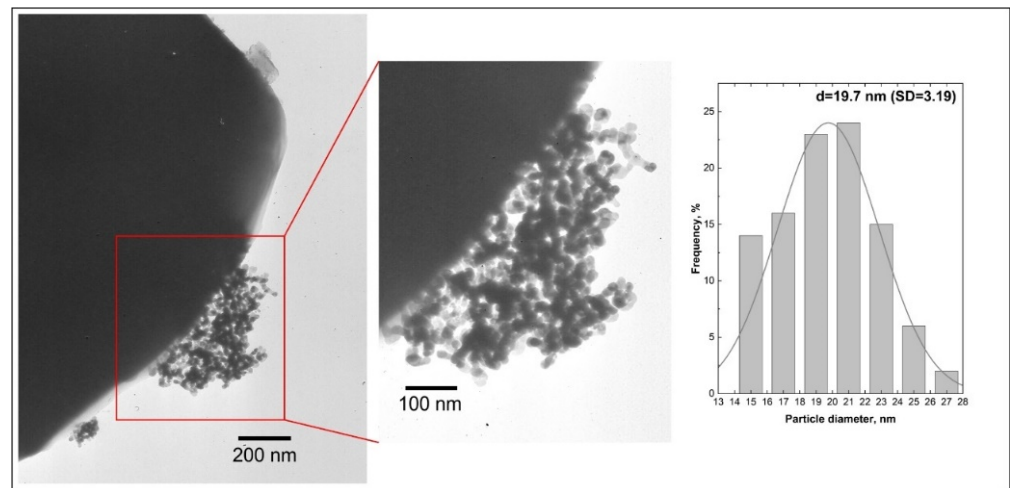
Similarly, for the Ru/Sil 0.1 XOH systems, we observe a decrease in basicity and Ru dispersion in the order of:



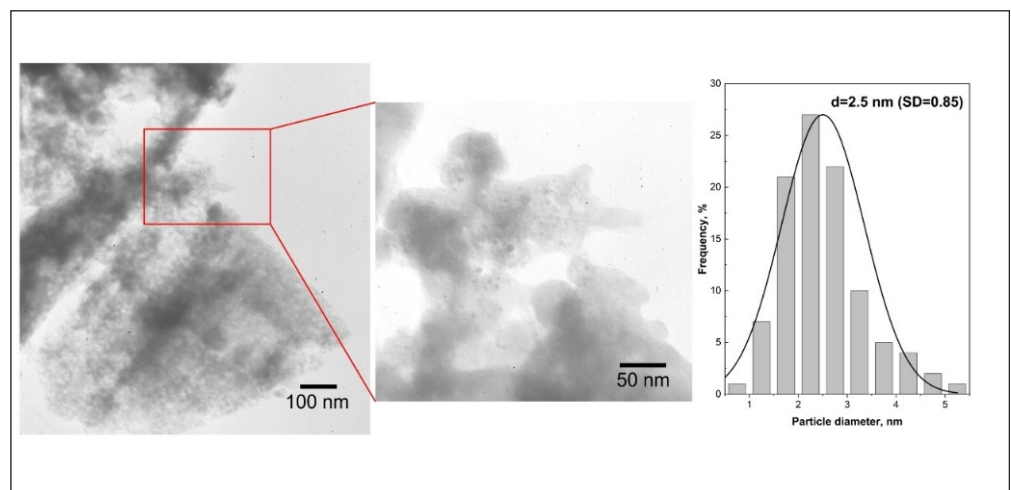
Another factor influencing dispersion was the specific surface area (SSA). The catalysts Ru/Sil-0.1 NaOH and Ru/Sil-0.1 KOH had the highest specific surface areas, while the catalysts with supports modified with high-concentration alkali solution possess much lower surface areas. This indicates that the mesoporous structure and large SSA of the modified supports significantly affect metal dispersion.

The changes in mean Ru particle size were characterized by TEM imaging. Representative images and the resulting particle size distributions (counted for at least 100 particles) are presented in Figure 9a–c for Ru/Sil (Figure 9a), Ru/Sil-01 NaOH (Figure 9b), and Ru/Sil-01 KOH (Figure 9c) catalysts, respectively. The darkest circular areas correspond to ruthenium particles due to the higher atomic number of Ru, with respect to other elements in the silicalite-1. Larger particles are observed for the Ru/Sil catalysts compared to the catalysts with the supports that present sodium or potassium in their composition. These results confirm the data obtained by chemisorption analysis.

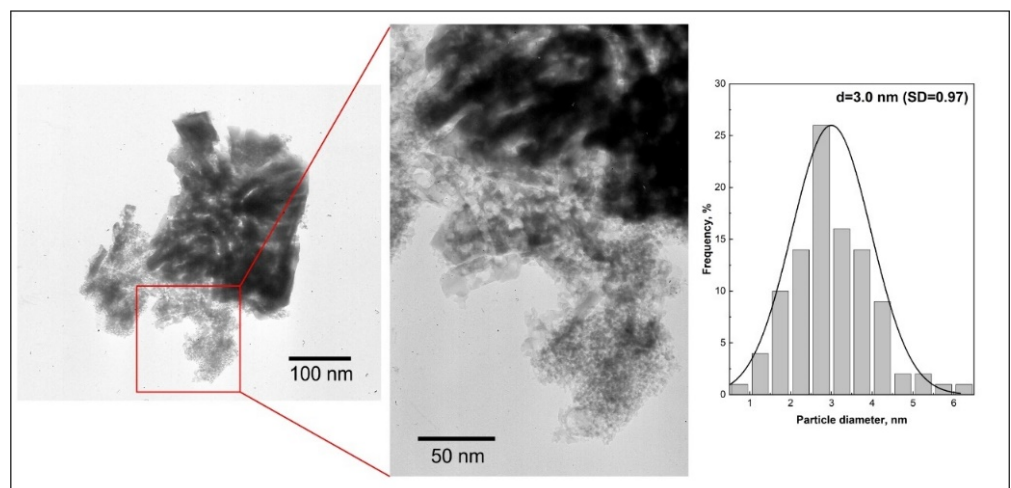
The catalytic activity of the obtained catalysts was examined in the hydrogenation of CO₂, and the comparison between the activity and the selectivity of ruthenium catalysts supported on unmodified and modified supports was discussed. The results of the catalytic tests performed at several temperatures in the presence of metals supported on different supports are presented in Figure 10a and the selectivity towards CH₄ in Figure 10b. The supports (Sil, Sil-0.1 XOH or Sil 1.0 XOH; X-K or Na) did not show any activity in the methanation of CO₂, while the reduced ruthenium catalysts were active in this process. Methane and CO were the only reaction products obtained over the tested catalysts.



(a)



(b)



(c)

Figure 9. TEM micrographs of different magnitude and particle size distribution for the Ru/Sil (a), Ru/Sil-0.1 NaOH (b), and Ru/Sil-0.1 KOH (c) catalysts.

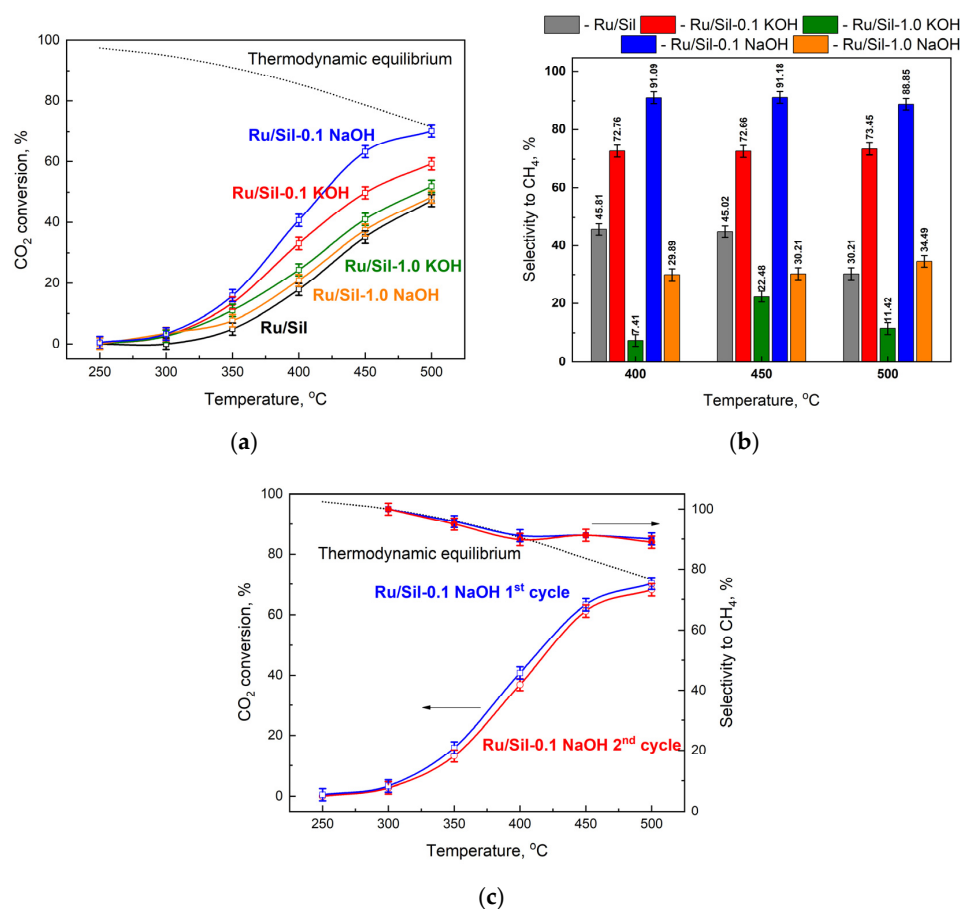


Figure 10. Catalytic activity tests: CO₂ conversion (a) and CH₄ selectivity (b) for the Ru catalysts, and catalytic stability of the Ru/Sil-0.1 NaOH catalyst (c). Reaction conditions: before reaction all catalysts (25 mg) were reduced in H₂ at 500 °C, 30 min; the feed gas composition—H₂:He:CO₂ = 4:5:1; total flow rate—100 cm³·min⁻¹.

Another important element of the response under study is the monitoring of carbon balance (CB). Carbon deposition theoretically does not occur if the H₂/CO₂ ratio is equal to or higher than the stoichiometric ratio [39]. Our studies were conducted at atmospheric pressure and at temperatures of up to 500 °C. Temperatures above 500 °C can cause sintering of Ru particles and increase carbon deposition, leading to catalyst deactivation. Thus, temperature control is vital as the exothermic methanation reaction can result in an apparent temperature increase in large-scale operations [40]. For this reason, the CB was monitored and was close to 1.0 at each temperature, meaning that there was no degradation of carbon dioxide.

The activity of all catalysts increases with increasing process temperature, reaching a maximum at 500 °C. Due to thermodynamic equilibrium, the reaction was not carried out at higher temperatures. The activity of the catalysts mainly depended on the type of support used. The lowest activities, over the whole temperature range, were observed for the Ru/Sil catalyst. The modification of silicalite-1 and its use as a support led to catalysts with activities higher than the starting Ru/Sil. The studied systems can be categorized into two groups depending on the concentration of the modifier. The use of supports modified with a 1.0 M solution of KOH or NaOH led to an increase in the activity of ruthenium catalysts, but the use of supports modified with lower concentration solutions (0.1 M) made it possible to obtain much more active catalysts. Among the systems tested, the Ru/Sil-0.1 NaOH catalyst showed the highest activity. For example, at 450 °C, its activity was 25% higher than that of Ru/Sil-0.1 KOH and almost twice as high as that of Ru/Sil-1.0 NaOH (Figure 10a).

A much greater effect of support modification was observed on selectivity toward methane—Figure 10b. While the starting catalyst (Ru/Sil) had a selectivity to CH₄ of 50% at 400 and 450 °C, using the supports modified with 1.0 M solutions resulted in a significant reduction in selectivity, especially for the Ru/Sil-1.0 KOH catalyst. Its selectivity was only ~7 and ~22% at 400 and 450 °C, respectively. Much better results were obtained for catalysts supported on the support modified with 0.1 M solutions. Thus, the highest selectivity of >90% was characterized by the most active Ru/Sil-0.1 NaOH catalysts.

For the most promising sample, Ru/Sil-0.1 NaOH, two cycles of reaction were conducted, in order to verify whether the increase in conversion and yield with the temperature was due to the first activation of the fresh catalyst or it can be considered as characteristic behavior of the reacting system, and thus obtainable on the spent catalyst also. The results of this test are reported in Figure 10c. As can be seen, the first and second cycles reported almost the same trend in CO₂ conversion and methane selectivity. This leads to two conclusions: firstly, the increase in the activity with the temperature rise is a characteristic trend of the system; secondly, no significant changes in the catalyst occur during the first cycle of reaction, thus demonstrating its stability, at least in the investigated reaction time.

The activity of the methanation catalysts was correlated with the concentration of the basic centers (Figure 11) and the dispersion and particle size of the active phase (Figure 12). This correlation is clearly visible in the case of our systems; an increase in total concentration of basic centers in the sample increases the total CO₂ methanation rate—Figure 11a,b.

In addition, the activity of the catalysts tested is correlated with the dispersion of the active phase. Figure 12a shows the dependence of apparent rate (r_t) and selectivity to CH₄ on ruthenium dispersion. The catalyst with the best dispersion (Ru/Sil-0.1 NaOH) shows the highest activity. This seems to be a logical conclusion because the high dispersion of ruthenium provides a large number of active centers. Moreover, the same catalyst is also the most selective to methane. Thus, from a practical point of view, the catalyst with the highest dispersion is the right choice.

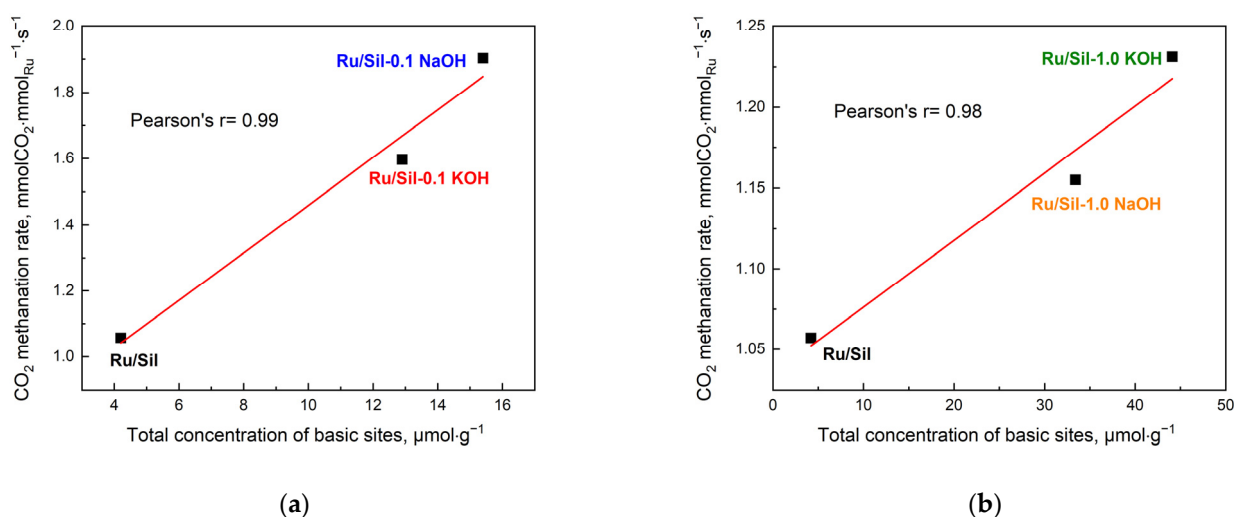


Figure 11. CO₂ methanation rate as a function of content of basic sites for Ru/Sil 0.1 XOH (a) and Ru/Sil 1.0 XOH (b) catalysts (X = Na or K). Reaction conditions: before reaction all catalysts (25 mg) were reduced in H₂ at 500 °C, 30 min; the feed gas composition—H₂:He:CO₂ = 4:5:1; total flow rate—100 cm³ min⁻¹; T_{reac} = 450 °C.

On the other hand, from a scientific point of view, it is interesting to study the intrinsic activity of metal crystallites of a specific size, which allows us to draw conclusions about the structural sensitivity of the CO₂ methanation reaction. Figure 12b shows the dependence of CO₂ methanation activity (expressed as TOF, s⁻¹) on ruthenium particle size at 450 °C. The activity of the investigated catalysts increased with the particle size of the active phase—Figure 12b. This means that higher activity is shown by ruthenium centers

located on large metal crystallites. However, the fact that there are far fewer of them (due to low dispersion) translates into lower overall activity. Similar correlations between turnover frequency of CO₂ conversion and the size of crystallites were shown by the authors of a paper [41] studying the effect of Ni crystallite size on the activity of CO₂ methanation.

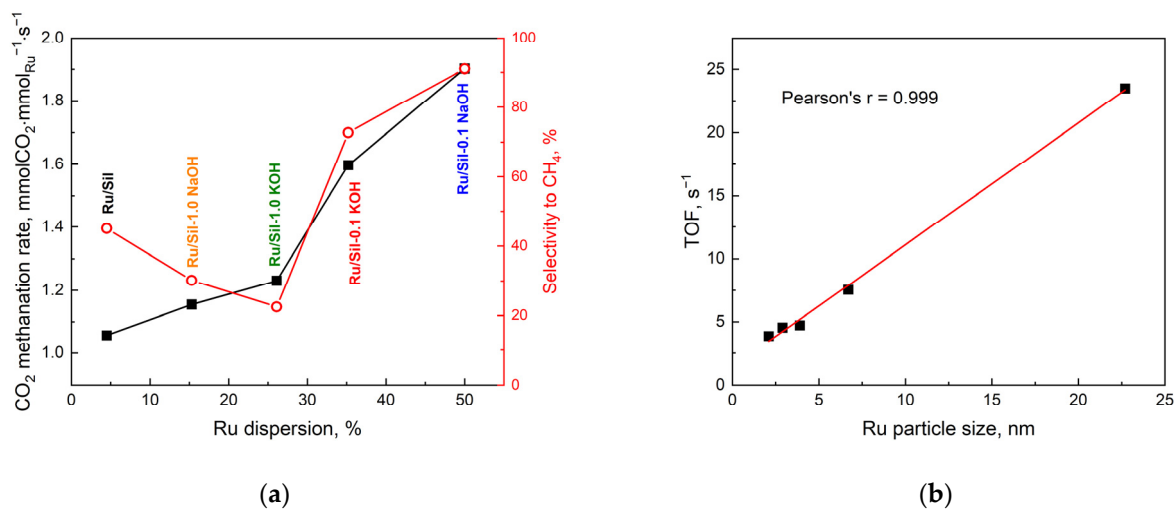


Figure 12. CO₂ methanation rate and selectivity CO₂ to CH₄ as a function of dispersion for ruthenium catalysts at $T_{\text{react.}} = 450\text{ }^{\circ}\text{C}$ (a) and the effect of Ru particle size on TOF (calculated by dividing the number of CO₂ molecules converted per second by the number of active (surface) Ru atoms) (b).

A comparison of the CO₂ methanation rate value obtained for the best Ru/Sil-0.1 NaOH catalyst ($536\text{ mmolCO}_2\cdot\text{g}_{\text{Ru}}^{-1}\cdot\text{h}^{-1}$; at $250\text{ }^{\circ}\text{C}$) with the results reported in the literature for ruthenium supported on Al₂O₃ ($470\text{ mmolCO}_2\cdot\text{g}_{\text{Ru}}^{-1}\cdot\text{h}^{-1}$) or MgO ($320\text{ mmolCO}_2\cdot\text{g}_{\text{Ru}}^{-1}\cdot\text{h}^{-1}$) [42], as well as ZrO₂ ($140\text{ mmolCO}_2\cdot\text{g}_{\text{Ru}}^{-1}\cdot\text{s}^{-1}$) [43], shows that our ruthenium catalyst supported on modified silicalite-1 is a more promising catalyst.

3. Materials and Methods

3.1. Preparation of Supports

Silicalite-1 (denoted as Sil) was synthesized according to the procedure described in [22,44]. The synthesized silicalite-1 was calcined at $550\text{ }^{\circ}\text{C}$ for 5 h in order to remove the template.

The calcined silicalite-1 was then modified with 0.1 M or 1.0 M solutions of alkali metal compounds (KOH (Stanlab) or NaOH (Chempur)). For this, 1 g of sample was mixed with 100 cm^3 of the respective alkali hydroxide aqueous solution. The mixture was stirred under reflux at $60\text{ }^{\circ}\text{C}$ for 1 h. Then, the samples were filtered, washed with deionized hot water, dried at $105\text{ }^{\circ}\text{C}$ for 24 h, and then calcined in air for 3 h at $550\text{ }^{\circ}\text{C}$. The resulting samples were labelled as Sil-XY, where X stands for the molar concentration of the used solution, and Y stands for the used inorganic compound (e.g., Sil-0.1 KOH was prepared with 0.1 M KOH solution).

3.2. Preparation of Catalysts

Ruthenium catalysts were prepared by an incipient wetness impregnation method using RuCl₃·nH₂O (Aldrich, St. Louis, MO, USA) solution as a metal precursor. The Ru content in the catalysts was 1 wt.%. An appropriate amount of support was placed in an aqueous solution of RuCl₃·nH₂O followed by evaporation. After that, the supports with the metal precursor were dried at $105\text{ }^{\circ}\text{C}$ for 24 h and reduced in a hydrogen flow for 2 h at $500\text{ }^{\circ}\text{C}$ for characterization (BET specific surface area, FT-IR, XRD, H₂ chemisorption, SEM, TEM, and TPD-CO₂).

3.3. Characterization

The supports, as well as the catalysts, were characterized by means of different techniques. X-ray powder diffraction patterns (XRD) were collected on a Philips Bruker D8 Advance diffractometer using Cu K α radiation ($\lambda = 1.54056 \text{ \AA}$) in the range of 2θ from 6° to 60° . FTIR spectra (KBr pellets) were obtained on a Bruker Tensor 27 spectrometer. The crystallinity (C_{IR}) of the initial and modified supports, as well as catalysts, was determined based on the intensity of the bands characteristic for the MFI structure (at 550 and 450 cm^{-1}) according to the formula [45]:

$$C_{IR} = \frac{I_{550}/I_{450}}{0.72} * 100\% \quad (5)$$

Scanning electron microscope (SEM) images were recorded on the Hitachi SU3500 microscope. Transmission electron microscopy (TEM) images were recorded on a JEOL 2000 microscope operating at an accelerating voltage of 80 kV . N_2 adsorption/desorption isotherms were measured at -196°C using a Micromeritics ASAP 2010 sorptometer. Prior to the measurement, the samples were outgassed under a vacuum at 275°C . The specific surface area was determined using the BET method, whereas the external surface area and micropore volume were calculated by the t-plot method. The total volume of pores was assessed using the single-point model (at $p/p_0 = 0.98$). The BJH pore size distributions were derived from the adsorption branch. Ruthenium content in catalysts reduced at 500°C for 2 h was determined by inductively coupled plasma optical emission spectroscopy (ICP-OES) on a Varian Vista-MPX spectrometer.

Measurements of temperature-programmed reduction with hydrogen (TPR- H_2) and temperature-programmed desorption of carbon dioxide (TPD- CO_2) were carried out on a Pulse ChemiSorb 2705 (Micromeritics) instrument. H_2 -TPR measurements were performed under a flow of $10 \text{ vol. \% H}_2/\text{Ar}$ ($20 \text{ cm}^3 \text{ min}^{-1}$ (99.999%, Linde, Pullach im Isartal, Germany)) from 50 to 550°C at a constant heating rate ($10^\circ \text{ min}^{-1}$). The hydrogen consumption was monitored with a thermal conductivity detector (TCD) and the signal was normalized to the same sample weight of 100 mg . In the TPR- H_2 studies, a quartz sand (Aldrich) impregnated with a ruthenium precursor was used as a reference material. The products of the reduction were retained by an isopropanol/liquid nitrogen cold trap at about -70°C . Prior to the TPD- CO_2 measurements, about 100 mg of the sample was pretreated in helium (He, 99.999, Aldrich) at 450°C for 30 min , then cooled down to 50°C and afterward saturated with carbon dioxide (CO_2 , 99.999, Aldrich) for 60 min . The physically adsorbed CO_2 was removed by purging with a helium flow at 50°C for 60 min and then the TPD analysis was carried out. All TPD- CO_2 profiles presented in this work were collected in the temperature range of 50 – 450°C with a heating rate of $10^\circ \text{ min}^{-1}$ and normalized to the same sample weight (100 g).

Hydrogen chemisorption measurements on supported metal catalysts were conducted by the static method at 100°C on a Micromeritics ASAP 2010C sorptometer. Prior to hydrogen chemisorption, freshly dried catalysts were reduced with H_2 (99.999%, Linde) at 500°C for 30 min , and then the catalyst samples were pretreated in situ to purify their surfaces from adsorbed gases. The pretreatment consisted of evacuation at room temperature for 15 min . and then at 350°C for 60 min ., followed by a reduction in hydrogen flow ($40 \text{ cm}^3 \cdot \text{min}^{-1}$) at 350°C for 60 min . and evacuation at 350°C for 120 min . Chemisorption of hydrogen was carried out at 100°C and the isotherms were determined using 5 different pressures in the range of 50 – 310 mmHg . Assuming the stoichiometry of one hydrogen atom per one surface ruthenium atom (Ru_s), the dispersion of ruthenium (D) can be expressed as $D = \text{Ru}_s/\text{Ru}_t = \text{H}/\text{Ru}_t$ (where Ru_t —total number of ruthenium atoms in the sample).

Prior to the reaction of CO_2 methanation, the samples were reduced with H_2 at 500°C for 30 min . The activity tests were performed with a feed stream containing CO_2 and H_2 in a stoichiometric ratio of $1:4$, along with He in order to achieve $1:1$ reactants:He dilution. Thus, the final feed stream ratio was $\text{H}_2:\text{He}:\text{CO}_2 = 4:5:1$ and the total flow rate was

100 cm³ min⁻¹ (all gases—99.999%, Linde). The mass of catalyst used in these experiments was typically 25 mg. The catalytic performance for the CO₂ hydrogenation reaction was evaluated using a fixed-bed reactor operating at atmospheric pressure in the temperature range of 250–500 °C. It should be noted that the reaction was carried out for 30 min at each temperature to achieve steady-state conditions. Gaseous reagents and products were measured every 50 °C with a chromatograph SRI Multiple Gas Analyzer #1 GC, equipped with a Silica Gel packed column, a Molecular Sieve 13X, and TCD detector, operating with He as the carrier gas. The CO₂ conversion (X_{CO_2}) was calculated using the expression (6):

$$X_{CO_2} = \frac{C_{CO,out} + C_{CH_4,out}}{C_{CO_2,out} + C_{CO,out} + C_{CH_4,out}} * 100 \quad (6)$$

where $C_{CO,out}$, $C_{CO_2,out}$ and $C_{CH_4,out}$ are the concentrations of CO, CO₂, and CH₄ in the outlet of the reactor.

Selectivities toward CH₄ (S_{CH_4}) and CO (S_{CO}) were calculated according to the expressions (7) and (8), respectively:

$$S_{CH_4} = \frac{C_{CH_4,out}}{C_{CH_4,out} + C_{CO,out}} * 100 \quad (7)$$

$$S_{CO} = \frac{C_{CO,out}}{C_{CH_4,out} + C_{CO,out}} * 100 \quad (8)$$

where $C_{CH_4,out}$ and $C_{CO,out}$ are the outlet concentrations of CH₄ and CO, respectively.

Carbon balance was calculated according to the expressions (9):

$$\text{Carbon balance (CB)} = \frac{C_{CH_4,out} + C_{CO_2,out} + C_{CO,out}}{C_{CO_2,in}} \quad (9)$$

where $C_{CH_4,out}$, $C_{CO_2,out}$, and $C_{CO,out}$ are the outlet concentrations of CH₄, CO₂, and CO, respectively and $C_{CO_2,in}$ is the concentrations of CO₂ in the inlet the reactor.

4. Conclusions

In this study, we investigated the impact of basicity and textural properties of silicalite-1 modified with alkali compound (NaOH and KOH) supports on the activity of ruthenium catalysts in the hydrogenation of carbon dioxide to methane. We determined the effect of modifier type and concentration on the structure and basicity of the final supports. The use of 1.0 M solutions of KOH or NaOH enhances the basicity of the supports while diminishing their surface area. Conversely, employing a lower concentrated solution (0.1 M) leads to increased porosity of the supports and generates sufficient basicity for catalytic activity. The use of KOH solutions caused deeper changes of textural properties and basicity than the use of NaOH solutions. The use of supports with appropriate porosity and basicity positively affects the reducibility and dispersion of the active phase. Ru/Sil-0.1 KOH and Ru/Sil-0.1 NaOH catalysts exhibit easier reducibility, with the dispersion of the active phase being significantly better compared to the dispersion of catalysts obtained by using systems modified with 1.0 M solutions or the initial silicalite-1 (Ru/Sil).

The application of modified silicalite-1 as supports for the ruthenium phase allows for the creation of a new category of catalyst, characterized by high activities and selectivity in the hydrogenation of CO₂ to CH₄, surpassing those of the ruthenium system supported on unmodified silicalite-1. This activity correlates with the basicity and surface area of the catalyst supports, influencing not only the size of the ruthenium particles but also the efficiency of CO₂ hydrogenation. Moreover, increasing the support's basicity (Sil-1.0 NaOH or Sil-1.0 KOH) causes a shift in hydrogenation selectivity towards CO. The ruthenium catalyst supported on silicalite-1 modified with 0.1 M NaOH (Ru/Sil-0.1 NaOH) demonstrates excellent catalytic properties for the hydrogenation of CO₂ to CH₄.

The obtained results indicate that the combination of basic and structural properties of the supports enables the tailoring of selectivity towards desired reaction products. Ruthenium catalysts on modified silicalite-1 supports exhibit significant potential in carbon dioxide hydrogenation reactions.

Author Contributions: Conceptualization, M.Z. and E.J.; Methodology, E.J. and M.Z.; Investigation, M.Z., E.J., A.D. and M.P.; Writing—original draft preparation, M.Z. and E.J.; Writing—review and editing, M.Z., E.J. and M.P.; Supervision, M.Z.; Visualization, M.Z., M.P. and E.J. All authors have read and agreed to the published version of the manuscript.

Funding: This research received no external funding.

Institutional Review Board Statement: Not applicable.

Informed Consent Statement: Not applicable.

Data Availability Statement: The data presented in this study are available on request from the corresponding author.

Conflicts of Interest: The authors declare no conflict of interest. The funders had no role in the design of the study; in the collection, analyses, or interpretation of data; in the writing of the manuscript, or in the decision to publish the results.

Sample Availability: Not applicable.

References

1. Meylan, F.D.; Moreau, V.; Erkman, S. Material constraints related to storage of future European renewable electricity surpluses with CO₂ methanation. *Energy Policy* **2016**, *94*, 366–376. [[CrossRef](#)]
2. Sabatier, P.; Senderens, J.B. New synthesis of methane. *J. Chem. Soc.* **1902**, *82*, 333.
3. Su, X.; Xu, J.; Liang, B.; Duan, H.; Hou, B.; Huang, Y. Catalytic carbon dioxide hydrogenation to methane: A review of recent studies. *J. Energy Chem.* **2016**, *25*, 553–565. [[CrossRef](#)]
4. Petala, A.; Panagiotopoulou, P. Methanation of CO₂ over alkali-promoted Ru/TiO₂ catalysts: I. Effect of alkali additives on catalytic activity and selectivity. *Appl. Catal. B* **2018**, *224*, 919–927. [[CrossRef](#)]
5. Wang, F.; Zhang, S.; Li, C.; Liu, J.; He, S.; Zhao, Y.; Yan, H.; Wei, M.; Evans, D.G.; Duan, X. Catalytic behavior of supported Ru nanoparticles on the (101) and (001) facets of anatase TiO₂. *RSC Adv.* **2014**, *4*, 10834–10840. [[CrossRef](#)]
6. Wang, W.; Wang, S.; Ma, X.; Gong, J. Recent advances in catalytic hydrogenation of carbon dioxide. *Chem. Soc. Rev.* **2011**, *40*, 3703–3727. [[CrossRef](#)]
7. Sharma, S.; Hu, Z.; Zhang, P.; McFarland, E.W.; Metiu, H. CO₂ methanation on Ru-doped ceria. *J. Catal.* **2011**, *278*, 297–309. [[CrossRef](#)]
8. Karelovic, A.; Ruiz, P. Mechanistic study of low temperature CO₂ methanation over Rh/TiO₂ catalysts. *J. Catal.* **2013**, *301*, 141–153. [[CrossRef](#)]
9. Darensbourg, D.J.; Ovalles, C.; Bauch, C.G. Mechanistic aspects of catalytic carbon dioxide methanation. *Rev. Inorg. Chem.* **1985**, *7*, 315–339. [[CrossRef](#)]
10. Wang, X.; Hong, Y.; Shi, H.; Szanyi, J. Kinetic modeling and transient DRIFTS–MS studies of CO₂ methanation over Ru/Al₂O₃ catalysts. *J. Catal.* **2016**, *343*, 185–195. [[CrossRef](#)]
11. Wang, F.; He, S.; Chen, H.; Wang, B.; Zheng, L.; Wei, M.; Evans, D.G.; Duan, X. Active Site Dependent Reaction Mechanism over Ru/CeO₂ Catalyst toward CO₂ Methanation. *J. Am. Chem. Soc.* **2016**, *138*, 6298–6305. [[CrossRef](#)] [[PubMed](#)]
12. Garbarino, G.; Bellotti, D.; Finocchio, E.; Magistri, L.; Busca, G. Methanation of carbon dioxide on Ru/Al₂O₃: Catalytic activity and infrared study. *Catal. Today* **2016**, *277 Pt 1*, 21–28. [[CrossRef](#)]
13. Duyar, M.S.; Treviño, M.A.A.; Farrauto, R.J. Dual function materials for CO₂ capture and conversion using renewable H₂. *Appl. Catal. B* **2015**, *168–169*, 370–376. [[CrossRef](#)]
14. Zheng, Q.; Farrauto, R.; Chau Nguyen, A. Adsorption and methanation of flue gas CO₂ with dual functional catalytic materials: A parametric study. *Ind. Eng. Chem. Res.* **2016**, *55*, 6768–6776. [[CrossRef](#)]
15. Hu, X.; Lu, G. Inhibition of methane formation in steam reforming reactions through modification of Ni catalyst and the reactants. *Green Chem.* **2009**, *11*, 724–732. [[CrossRef](#)]
16. Campbell, T.K.; Falconer, J.L. Carbon dioxide hydrogenation on potassium-promoted nickel catalysts. *Appl. Catal.* **1989**, *50*, 189–197. [[CrossRef](#)]
17. Panagiotopoulou, P. Methanation of CO₂ over alkali-promoted Ru/TiO₂ catalysts: II. Effect of alkali additives on the reaction pathway. *Appl. Catal. B* **2018**, *236*, 162–170. [[CrossRef](#)]
18. Li, D.; Ichikuni, N.; Shimazu, S.; Uematsu, T. Catalytic properties of sprayed Ru/Al₂O₃ and promoter effects of alkali metals in CO₂ hydrogenation. *Appl. Catal. A* **1998**, *172*, 351–358. [[CrossRef](#)]

19. Cimino, S.; Boccia, F.; Lisi, L. Effect of alkali promoters (Li, Na, K) on the performance of Ru/Al₂O₃ catalysts for CO₂ capture and hydrogenation to methane. *J. CO₂ Util.* **2020**, *37*, 195–203. [[CrossRef](#)]
20. Solymosi, F.; Tombácz, I.; Koszta, J. Effects of variation of electric properties of TiO₂ support on hydrogenation of CO and CO₂ over Rh catalysts. *J. Catal.* **1985**, *95*, 578–586. [[CrossRef](#)]
21. Guo, M.; Lu, G. The difference of roles of alkaline-earth metal oxides on silica-supported nickel catalysts for CO₂ methanation. *RSC Adv.* **2014**, *4*, 58171–58177. [[CrossRef](#)]
22. Janiszewska, E.; Kowalska-Kuś, J.; Góra-Marek, K.; Szymocha, A.; Nowińska, K.; Kowalak, S. Modification of silicalite-1 with ammonium compounds aimed at preparation of acidic catalyst for acetalization of glycerol with acetone. *Appl. Catal. A* **2019**, *581*, 1–10. [[CrossRef](#)]
23. Guo, Y.-P.; Wang, H.-J.; Guo, Y.-J.; Guo, L.-H.; Chu, L.-F.; Guo, C.-X. Fabrication and characterization of hierarchical ZSM-5 zeolites by using organosilanes as additives. *J. Chem. Eng.* **2011**, *166*, 391–400. [[CrossRef](#)]
24. Schmidt, W.; Wilczok, U.; Weidenthaler, C.; Medenbach, O.; Goddard, R.; Buth, G.; Cepak, A. Preparation and morphology of pyramidal MFI single-crystal segments. *J. Phys. Chem. B* **2007**, *111*, 13538–13543. [[CrossRef](#)]
25. Lamberti, C.; Bordiga, S.; Zecchina, A.; Artioli, G.; Marra, G.; Spano, G. Ti Location in the MFI Framework of Ti-Silicalite-1: A Neutron Powder Diffraction Study. *J. Am. Chem. Soc.* **2001**, *123*, 2204–2212. [[CrossRef](#)]
26. Navarro-Jaén, S.; Navarro, J.C.; Bobadilla, L.F.; Centeno, M.A.; Laguna, O.H.; Odriozola, J.A. Size-tailored Ru nanoparticles deposited over γ -Al₂O₃ for the CO₂ methanation reaction. *Appl. Surf. Sci.* **2019**, *483*, 750–761. [[CrossRef](#)]
27. Jonas, H.; Jareman, F. Texture of MFI films grown from seeds. *Curr. Opin. Colloid Interface Sci.* **2005**, *10*, 226–232. [[CrossRef](#)]
28. Tarach, K.A.; Góra-Marek, K.; Martínez-Triguero, J.; Melián-Cabrera, I. Acidity and accessibility studies of desilicated ZSM-5 zeolites in terms of their effectiveness as catalysts in acid-catalyzed cracking processes. *Catal. Sci. Technol.* **2017**, *7*, 858–873. [[CrossRef](#)]
29. Tao, Y.; Kanoh, H.; Kaneko, K. Comment: Questions Concerning the Nitrogen Adsorption Data Analysis for Formation of Supermicropores in ZSM-5 Zeolites. *Adv. Mater.* **2005**, *17*, 2789–2792. [[CrossRef](#)]
30. Sun, H.; Zhang, Y.; Guan, S.; Huang, J.; Wu, C. Direct and highly selective conversion of captured CO₂ into methane through integrated carbon capture and utilization over dual functional materials. *J. CO₂ Util.* **2020**, *38*, 262–272. [[CrossRef](#)]
31. Gao, J.; Hou, Z.; Guo, J.; Zhu, Y.; Zheng, X. Catalytic conversion of methane and CO₂ to synthesis gas over a La₂O₃-modified SiO₂ supported Ni catalyst in fluidized-bed reactor. *Catal. Today* **2008**, *131*, 278–284. [[CrossRef](#)]
32. Proaño, L.; Tello, E.; Arellano-Trevino, M.A.; Wang, S.; Farrauto, R.J.; Cobo, M. In-situ DRIFTS study of two-step CO₂ capture and catalytic methanation over Ru, “Na₂O”/Al₂O₃ dual functional material. *Appl. Surf. Sci.* **2019**, *479*, 25–30. [[CrossRef](#)]
33. Koopman, P.G.J.; Kieboom, A.P.G.; van Bekkum, H. Characterization of ruthenium catalysts as studied by temperature programmed reduction. *J. Catal.* **1981**, *69*, 172–179. [[CrossRef](#)]
34. Betancourt, P.; Rives, A.; Hubaut, R.; Scott, C.E.; Goldwasser, J. A study of the ruthenium–alumina system. *Appl. Catal.* **1998**, *170*, 307–314. [[CrossRef](#)]
35. Mazziere, V.; Coloma-Pascual, F.; Arcoya, A.; L’Argentièrre, P.C.; Fígoli, N.S. XPS, FTIR and TPR characterization of Ru/Al₂O₃ catalysts. *Appl. Surf. Sci.* **2003**, *210*, 222–230. [[CrossRef](#)]
36. Esen, M.; Akmaz, S.; Naci Koç, S.; Ali Gürkaynak, M. The hydrogenation of 5-hydroxymethylfurfural (HMF) to 2,5-dimethylfuran (DMF) with sol–gel Ru-Co/SiO₂ catalyst. *J. Solgel. Sci. Technol.* **2019**, *91*, 664–672. [[CrossRef](#)]
37. Zieliński, M.; Pietrowski, M.; Kiderys, A.; Ko, M.; Alwin, E. A comparative study of the performance of Pt/MgF₂, Ir/MgF₂ and Ru/MgF₂ catalysts in hydrogenation reactions. *J. Fluorine Chem.* **2017**, *195*, 18–25. [[CrossRef](#)]
38. Miyazaki, E. Chemisorption of diatomic molecules (H₂, N₂, CO) on transition d- metals. *J. Catal.* **1980**, *65*, 84–94. [[CrossRef](#)]
39. Gao, J.; Wang, Y.; Ping, Y.; Hu, D.; Xu, G.; Gu, F.; Su, F. A thermodynamic analysis of methanation reactions of carbon oxides for the production of synthetic natural gas. *RSC Adv.* **2012**, *2*, 2358–2368. [[CrossRef](#)]
40. Jürgensen, L.; Ehimen, E.A.; Born, J.; Holm-Nielsen, J.B. Dynamic biogas upgrading based on Sabatier process: Thermodynamic and dynamic process simulation. *Bioresour. Technol.* **2015**, *178*, 323–329. [[CrossRef](#)]
41. Marconi, E.; Tuti, S.; Luisetto, I. Structure-Sensitivity of CO₂ Methanation over Nanostructured Ni Supported on CeO₂ Nanorods. *Catalysts* **2019**, *9*, 375. [[CrossRef](#)]
42. Kowalczyk, Z.; Stołcki, K.; Raróg-Pilecka, W.; Miśkiewicz, E.; Wilczkowska, E.; Karpiński, Z. Supported ruthenium catalysts for selective methanation of carbon oxides at very low CO_x/H₂ ratios. *Appl. Catal. A* **2008**, *342*, 35–39. [[CrossRef](#)]
43. Chen, S.; Abdel-Mageed, A.M.; Li, M.; Cisneros, S.; Bansmann, J.; Rabeah, J.; Brückner, A.; Groß, A.; Behm, R.J. Electronic metal-support interactions and their promotional effect on CO₂ methanation on Ru/ZrO₂ catalysts. *J. Catal.* **2021**, *400*, 407–420. [[CrossRef](#)]
44. Zieliński, M.; Kot, M.; Pietrowski, M.; Wojcieszak, R.; Kowalska-Kuś, J.; Janiszewska, E. Studies of new Iridium catalysts supported on modified silicalite-1—Their structure and hydrogenating properties. *Materials* **2021**, *14*, 4465. [[CrossRef](#)]
45. Koekkoek, A.J.J.; Xin, H.; Yang, Q.; Li, C.; Hensen, E.J.M. Hierarchically structured Fe/ZSM-5 as catalysts for the oxidation of benzene to phenol. *Micropor. Mesopor. Mat.* **2011**, *145*, 172–181. [[CrossRef](#)]

Disclaimer/Publisher’s Note: The statements, opinions and data contained in all publications are solely those of the individual author(s) and contributor(s) and not of MDPI and/or the editor(s). MDPI and/or the editor(s) disclaim responsibility for any injury to people or property resulting from any ideas, methods, instructions or products referred to in the content.